

# Contrastive Quantization with Code Memory for Unsupervised Image Retrieval

Jinpeng Wang<sup>1</sup>, Ziyun Zeng<sup>1</sup>, Bin Chen<sup>2\*</sup>, Tao Dai<sup>3</sup>, Shu-Tao Xia<sup>1</sup>

<sup>1</sup>Tsinghua University <sup>2</sup>Harbin Institute of Technology, Shenzhen <sup>3</sup>Shenzhen University

{wjp20, zengzy21}@mails.tsinghua.edu.cn, cb17@tsinghua.org.cn, daitao.edu@gmail.com, xiast@sz.tsinghua.edu.cn

## Abstract

The high efficiency in computation and storage makes hashing (including binary hashing and quantization) a common strategy in large-scale retrieval systems. To alleviate the reliance on expensive annotations, unsupervised deep hashing becomes an important research problem. This paper provides a novel solution to *unsupervised deep quantization*, namely **Contrastive Quantization with Code Memory (MeCoQ)**. Different from existing reconstruction-based strategies, we learn unsupervised binary descriptors by contrastive learning, which can better capture discriminative visual semantics. Besides, we uncover that *codeword diversity regularization* is critical to prevent contrastive learning-based quantization from model degeneration. Moreover, we introduce a novel *quantization code memory module* that boosts contrastive learning with lower feature drift than conventional feature memories. Extensive experiments on benchmark datasets show that MeCoQ outperforms state-of-the-art methods.

## Introduction

Hashing (Wang et al. 2017) plays a key role in Approximate Nearest Neighbor (ANN) search and has been widely applied in large-scale systems to improve search efficiency. There are two technical branches in hashing, namely binary hashing and quantization. Binary hashing methods (Charikar 2002; Heo et al. 2012) transform data into the Hamming space such that distances are measured quickly with bitwise operations. Quantization methods (Jegou, Douze, and Schmid 2010) divide real data space into disjoint cells. Then the data points in each cell are approximately represented as the centroid. Since the inter-centroid distances can be pre-computed as a lookup table, quantization methods can efficiently calculate pairwise distance.

With the progress in deep learning, the past few years have seen many deep hashing methods (Yuan et al. 2020; Liu et al. 2016) with impressive performance. Unfortunately, annotating tons of data in real-world applications is expensive, making it hard to apply these supervised methods. Recent research interests have arisen in unsupervised deep hashing to address this issue, but existing works are not satisfactory enough. On the one hand, most existing studies in unsupervised deep hashing focus on preserving the information from continuous features. They mostly use quantization loss (Lin

et al. 2016; Chen, Cheung, and Wang 2018) and similarity reconstruction loss (Shen et al. 2018) as the learning objectives, resulting in heavy reliance on the quality of extracted features from pre-trained backbones (Krizhevsky, Sutskever, and Hinton 2012; Simonyan and Zisserman 2015; He et al. 2016). If an adopted backbone generalizes poorly in the target domain, the unsatisfactory features will degrade the output binary codes fundamentally. On the other hand, Lin et al. (2016); Huang et al. (2017) introduced rotation invariance of images to learn deep hashing, but weak negative samples and ineffective training schemes led to inferior performance.

This paper focuses on *unsupervised deep quantization*. To make better use of unlabeled training data, we perform Contrastive Learning (CL) (Hadsell, Chopra, and LeCun 2006) that learns representations by mining visual-semantic invariance from inputs (Chen et al. 2020; He et al. 2020). CL has become a promising direction toward deep unsupervised representation, but CL-based deep quantization remains non-trivial. Specifically, we find three challenges in this task: **(i) Sampling bias.** Without label supervision, a randomly sampled batch may contain positive samples that are falsely taken as negatives. **(ii) Model degradation.** We observe that quantization codewords of the same codebook tend to get closer during CL, which gradually degrades the representation ability and harms the model. **(iii) The conflict between effect and efficiency in training.** CL benefits from a large batch size that ensures enough negative samples, while a single GPU can afford a limited batch size. Training by CL often requires multi-GPU synchronization, which is complex in engineering and less efficient. To improve the efficiency, some recent studies (Wu et al. 2018; Misra and Maaten 2020) enable small-batch CL by caching embeddings in a memory bank and reusing them as negatives in later iterations. However, as the encoder updates, the cached embeddings will expire and affect the effect of CL.

To tackle the problems, we propose **Contrastive Quantization with Code Memory (MeCoQ)** that combines memory-based CL and deep quantization in a *mutually beneficial* framework. Specifically, **(i) MeCoQ is bias-aware.** We adopt a debiased framework (Chuang et al. 2020) that can correct the sampling bias in CL. **(ii) MeCoQ avoids degeneration.** We find that codeword diversity is critical to prevent the CL-based quantization model from degeneration. Hence, we design a codeword regularization to reinforce MeCoQ. **(iii)**

\*Corresponding author.

*MeCoQ* boosts CL effectively and efficiently. We propose a novel memory bank for quantization codes that shows lower feature drift (Wang et al. 2020) than existing feature memories. Thus, it can retain cached negatives valid for a longer period and enhance the effect of CL, without heavy computations from the momentum encoder (He et al. 2020).

Our contributions can be summarized as follows.

- We provide a novel solution to unsupervised deep quantization, which combines contrastive learning and deep quantization in a mutually beneficial framework.
- We show that codeword diversity is critical to prevent contrastive deep quantization from model degeneration.
- We propose a quantization code memory to enhance the effect of memory-based contrastive learning.
- Extensive experiments on public benchmarks show that MeCoQ outperforms state-of-the-art methods.

## Related Work

**Unsupervised Hashing** Traditional unsupervised hashing includes binary hashing (Charikar 2002; Weiss, Torralba, and Fergus 2008; Salakhutdinov and Hinton 2009; Heo et al. 2012; Gong et al. 2012) and quantization (Jegou, Douze, and Schmid 2010; Ge et al. 2013; Zhang, Du, and Wang 2014; Morozov and Babenko 2019). Limited by the hand-designed representations (Oliva and Torralba 2001; Lowe 2004), these methods reach suboptimal performance.

Deep hashing methods with Convolutional Neural Networks (CNNs) (Krizhevsky, Sutskever, and Hinton 2012; Simonyan and Zisserman 2015; He et al. 2016) usually perform better than non-deep hashing methods. Existing deep hashing methods can be categorized into generative (Dai et al. 2017; Duan et al. 2017; Zieba et al. 2018; Song et al. 2018; Dizaji et al. 2018; Shen, Liu, and Shao 2019; Shen et al. 2020; Li and van Gemert 2021; Qiu et al. 2021) or discriminative (Lin et al. 2016; Huang et al. 2017; Su et al. 2018; Chen, Cheung, and Wang 2018; Yang et al. 2018, 2019; Tu, Mao, and Wei 2020) series. Most of them impose various constraints (*i.e.*, loss or regularization terms) such as pointwise constraints: **(i)** quantization error (Duan et al. 2017; Chen, Cheung, and Wang 2018), **(ii)** even bit distribution (Zieba et al. 2018; Shen, Liu, and Shao 2019), **(iii)** bit irrelevance (Dizaji et al. 2018), **(iv)** maximizing mutual information between features and codes (Li and van Gemert 2021; Qiu et al. 2021); and pairwise constraints: **(v)** preserving similarity among continuous feature vectors (Su et al. 2018; Yang et al. 2018, 2019; Tu, Mao, and Wei 2020). They merely explore statistical characteristics of hash codes or focus on preserving the semantic information from continuous features, which leads to heavy dependence on high-quality pre-trained features. Due to limited generalization ability, the adopted CNNs may extract unsatisfactory features for images from new domains, which harms generated hash codes fundamentally. On the other hand, DeepBit (Lin et al. 2016) and UTH (Huang et al. 2017) introduce rotation invariance of images to improve deep hashing. Unfortunately, rotation itself is not enough to construct informative negative samples and the training schemes of DeepBit and UTH are less effective, which leads to inferior performances. Most recently, Qiu et al. (2021) combined contrastive learning with

deep binary hashing. By taking effective data augmentations and engaging more negative samples, it shows promising results. Different from them, we explore the combination of contrastive learning and deep quantization that is more challenging. We propose a codeword diversity regularization to prevent model degeneration. Besides, we adopt a debiasing mechanism and propose a quantization code memory to enhance contrastive learning, yielding better results.

**Contrastive Learning** Contrastive Learning (CL) (Hadsell, Chopra, and LeCun 2006) based representation learning has drawn increasing attention. Wu et al. (2018) proposed an instance discrimination method that combines a non-parametric classifier (*i.e.*, a memory bank) with a cross-entropy loss (*aka* InfoNCE (Oord, Li, and Vinyals 2018) or contrastive loss (He et al. 2020)). Positive samples from the same image are pulled closer and negative samples from other images are pushed apart. The subsequent instance-wise CL methods focus on designing *end-to-end* (Chen et al. 2020), *memory bank*-based (Misra and Maaten 2020), or *momentum encoder*-based (He et al. 2020) architectures. Besides, cluster-wise contrastive methods (Caron et al. 2020; Li et al. 2021) integrate the clustering objective into CL, which shows promising results. Moreover, there are some works addressing sampling bias (Chuang et al. 2020) or exploring effective negative sampling (Robinson et al. 2021) in CL, which improve the training effect. We uncover that codeword diversity is critical to enable CL in deep quantization. Besides, we propose a novel memory that stores quantization codes. Interestingly, without needing a momentum encoder, it can show lower feature drift (Wang et al. 2020) than existing feature memories (Wu et al. 2018; Misra and Maaten 2020) and thus boosts CL effectively.

## Modeling Framework

### Problem Formulation and Model Overview

Given an unlabeled training set  $\mathcal{D}$  of  $N_{\mathcal{D}}$  images where each image  $\mathbf{x}$  can be flattened as a  $P$ -dimensional vector, the goal of unsupervised deep quantization is to learn a neural quantizer  $Q : \mathbb{R}^P \mapsto \{0, 1\}^B$  that encodes images as  $B$ -bit semantic quantization codes (*aka* the binary representations) for efficient image retrieval. To this end, we propose **Contrastive Quantization with Code Memory (MeCoQ)** in an end-to-end deep learning architecture. As shown in Figure 1, MeCoQ consists of: **(i)** Two operators sampled from the same data augmentation family ( $T \sim \mathcal{T}$  and  $T' \sim \mathcal{T}$ ), which are applied to each training image to obtain two correlated views ( $\mathbf{x}_q$  and  $\mathbf{x}_k \in \mathbb{R}^P$ ). **(ii)** A deep embedding module  $h$  combined with a standard CNN (Simonyan and Zisserman 2015) and a transform layer, which produces a continuous embedding  $\mathbf{z} \in \mathbb{R}^D$  for an input view  $\mathbf{x} \in \mathbb{R}^P$ . **(iii)** A trainable quantization module that produces a *soft* quantization code vector  $\mathbf{p} \in \mathbb{R}^B$  and the reconstruction  $\hat{\mathbf{z}} \in \mathbb{R}^D$  for  $\mathbf{z} \in \mathbb{R}^D$ . In inference, it directly outputs the *hard* quantization code vector  $\mathbf{b} \in \{0, 1\}^B$  for image  $\mathbf{x}$ . **(iv)** A code memory bank  $\mathcal{M}$  to cache the quantization code vectors of images, which serves as an additional source of negative training keys and is not involved in inference.

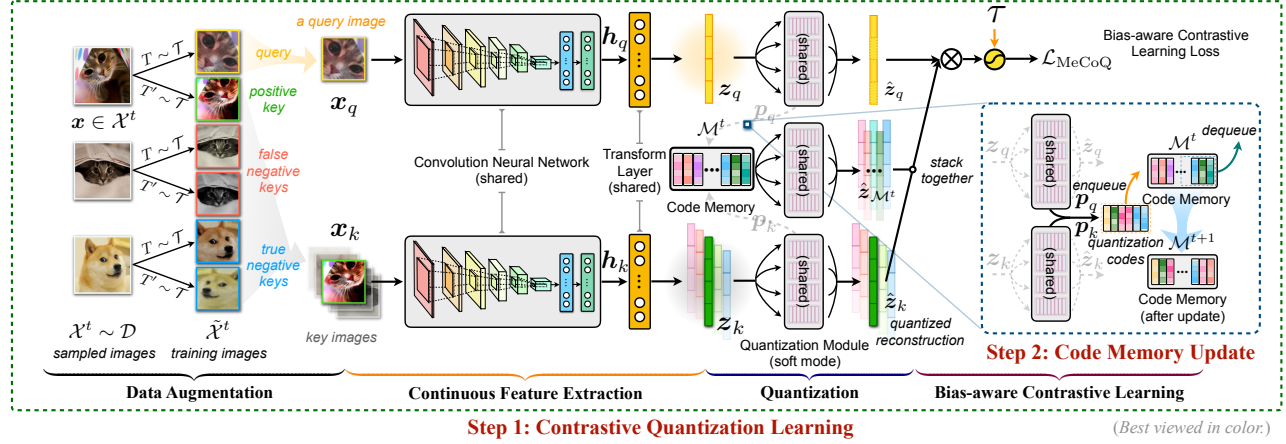


Figure 1: The framework of MeCoQ. After augmentation, we set one view for an image as the training *query*  $x_q$  and leave the other view  $x_k$  along with the views of other images as the *keys* in contrastive learning. Then, we extract the embeddings for these images and forward them to the quantization module to get quantized reconstructions. Embeddings reconstructed from the code memory bank serve as additional negative keys that boost contrastive learning. Next, we maximize the similarity between the query and the positive key (*i.e.*, the other view from the same image) and minimize the similarities of negative query-key pairs. Finally, we update the code memory bank with the quantization codes of the views of current image batch.

## Debiased Contrastive Learning for Quantization

**Trainable Quantization** It is hard to integrate traditional quantization (Jegou, Douze, and Schmid 2010) into the deep learning framework because the codeword assignment step is clustering-based and can not be trained by back-propagation. To enable end-to-end learning in MeCoQ, we apply a trainable quantization scheme. Denote the quantization codebooks as  $\mathcal{C} = \mathcal{C}^1 \times \mathcal{C}^2 \times \dots \times \mathcal{C}^M$ , where the  $m$ -th codebook  $\mathcal{C}^m \in \mathbb{R}^{K \times d}$  consists of  $K$  codewords  $\mathbf{c}_1^m, \mathbf{c}_2^m, \dots, \mathbf{c}_K^m \in \mathbb{R}^d$ . Assume that  $\mathbf{z} \in \mathbb{R}^D$  can be divided into  $M$  equal-length  $d$ -dimensional segments, *i.e.*,  $\mathbf{z} \in \mathbb{R}^D \equiv [\mathbf{z}^1, \dots, \mathbf{z}^M]$ ,  $\mathbf{z}^m \in \mathbb{R}^d$ ,  $d = D/M$ ,  $1 \leq m \leq M$ . Given a vector, each codebook is used to quantize one segment respectively. In the  $m$ -th  $d$ -dimensional subspace, the segment and codewords are first normalized:

$$\mathbf{z}^m \leftarrow \mathbf{z}^m / \|\mathbf{z}^m\|_2, \mathbf{c}_i^m \leftarrow \mathbf{c}_i^m / \|\mathbf{c}_i^m\|_2. \quad (1)$$

Then each segment is quantized with codebook attention by

$$\hat{\mathbf{z}}^m = \text{Attention}(\mathbf{z}^m, \mathcal{C}^m, \mathcal{C}^m) = \sum_{i=1}^K p_i^m \mathbf{c}_i^m, \quad (2)$$

where attention score  $p_i^m$  is computed with the  $\alpha$ -softmax:

$$p_i^m = \text{softmax}_\alpha \left( \mathbf{z}^{m\top} \mathbf{c}_i^m \right) = \frac{\exp(\alpha \cdot \mathbf{z}^{m\top} \mathbf{c}_i^m)}{\sum_{j=1}^K \exp(\alpha \cdot \mathbf{z}^{m\top} \mathbf{c}_j^m)}. \quad (3)$$

The  $\alpha$ -softmax is a differentiable alternative to the argmax that relaxes the discrete optimization of hard codeword assignment to a trainable form. Finally, we get *soft* quantization code and the *soft* quantized reconstruction of  $\mathbf{z}$  as

$$\mathbf{p} = \text{concatenate}(\mathbf{p}^1, \mathbf{p}^2, \dots, \mathbf{p}^M) \in \mathbb{R}^{KM} \equiv \mathbb{R}^B, \quad (4)$$

$$\hat{\mathbf{z}} = \text{concatenate}(\hat{\mathbf{z}}^1, \hat{\mathbf{z}}^2, \dots, \hat{\mathbf{z}}^M). \quad (5)$$

**Debiased Contrastive Learning** We conduct Contrastive Learning (CL) based on the soft quantized reconstruction vectors. Because negative keys for a training query are randomly sampled from unlabeled training set, there are unavoidably some *false-negative* keys that harm CL. To tackle this problem, we adopt a bias-aware framework (Chuang et al. 2020). The debiased CL loss is defined as

$$\mathcal{L}_{\text{DCL}} = - \sum_{q=1}^{2N} \log \frac{\exp(\frac{s_{q,k^+}}{\tau})}{\exp(\frac{s_{q,k^+}}{\tau}) + \mathcal{N}_{\text{In-Batch}}}, \quad (6)$$

where  $N$  is the batch size,  $q$  and  $k^+$  denote the indices of the training query and the positive key in the augmented batch,  $\tau$  is the temperature hyper-parameter. The similarity between a query  $q$  and a key  $k$  is defined as  $s_{q,k} \triangleq \hat{\mathbf{z}}_q^\top \hat{\mathbf{z}}_k$ . The debiased in-batch negative term in Eq.(6) is defined as

$$\mathcal{N}_{\text{In-Batch}} \triangleq \sum_{\substack{k^-=1, \\ k^- \notin \{q, k^+\}}}^{2N} \left[ \frac{\exp(\frac{s_{q,k^-}}{\tau})}{1 - \rho^+} - \frac{\rho^+ \cdot \exp(\frac{s_{q,k^+}}{\tau})}{1 - \rho^+} \right], \quad (7)$$

where  $k^-$  denotes the indices of negative key and  $\rho^+$  is the positive prior for bias correction.

## Regularization to Avoid Model Degeneration

**Model Degeneration** We find that deep quantization is prone to degenerate as CL goes on. To show the issue, we reduce irrelevant factors<sup>1</sup> and train a simplified 32-bit MeCoQ by vanilla CL on the Flickr25K dataset. As shown in Figure 2(a), the model performance (solid red line) declines while the loss (dash red line) rises with fluctuation. It seems

<sup>1</sup>We have done pretest about the effect of debiasing mechanism to the issue. As the results showed that it does not change the phenomenon, we exclude it for a concise interpretation in this section.

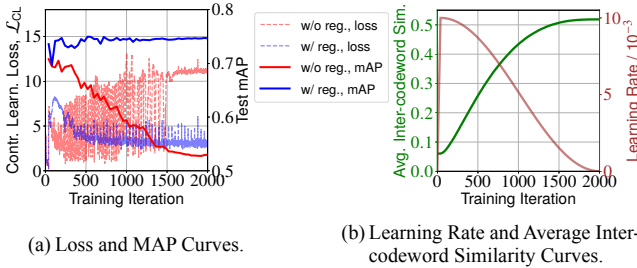


Figure 2: MeCoQ degenerates during contrastive learning because codewords in the same codebook are getting closer. The codeword diversity regularization can avoid it.

that the success of CL for continuous representation doesn't generalize to quantization directly. Considering the difference in models, we investigate the behavior of quantization codebooks during CL. Intuitively, we observe the changes of average inter-codeword similarity, namely,

$$\Omega_C = \frac{1}{MK^2} \sum_{m=1}^M \sum_{i=1}^K \sum_{j=1}^K \mathbf{c}_i^m \top \mathbf{c}_j^m. \quad (8)$$

Figure 2(b) shows a monotonic increase of  $\Omega_C$ , which slows down as the learning rate decreases. It suggests that the optimization leads to a degenerated solution.

Here we discuss what may cause this phenomenon. Recall that vanilla CL loss *w.r.t.* a training query  $\mathbf{x}_q$  is

$$\mathcal{L}_{\text{CL}}(\mathbf{x}_q) = -\log \frac{\exp(\frac{s_{q,k^+}}{\tau})}{\exp(\frac{s_{q,k^+}}{\tau}) + \sum_{\substack{k^- = 1, \\ k^- \notin \{q, k^+\}}}^{2N} \exp(\frac{s_{q,k^-}}{\tau})}. \quad (9)$$

**Proposition 1.** Suppose that  $\mathbf{x}_{k^+}$  is the positive training key and  $\mathbf{x}_{k^-}$  is a negative key to  $\mathbf{x}_q$ .  $\hat{\mathbf{z}}_{k^+}$  and  $\hat{\mathbf{z}}_{k^-}$  are the reconstructed embeddings *w.r.t.*  $\mathbf{x}_{k^+}$  and  $\mathbf{x}_{k^-}$ , then we have

$$\left\| \frac{\partial \mathcal{L}_{\text{CL}}(\mathbf{x}_q)}{\partial \hat{\mathbf{z}}_{k^+}} \right\| > \left\| \frac{\partial \mathcal{L}_{\text{CL}}(\mathbf{x}_q)}{\partial \hat{\mathbf{z}}_{k^-}} \right\| > 0. \quad (10)$$

We proof Proposition 1 in Appendix. It suggests that the scale of loss gradient *w.r.t.* the positive key is greater than that *w.r.t.* any negative key. Engaging more negatives leads to a larger gap between such scales. Besides, to reduce the deviation between soft quantization in training and hard quantization in inference, we take a relatively large  $\alpha$  (10 by default) in the codeword attention (Eq.(2)). It makes each soft reconstruction and assigned codeword approximate at the forward step. In the back-propagation, their gradients are also approximate. Thus, it can hold when replacing  $\hat{\mathbf{z}}_{k^+}$  and  $\hat{\mathbf{z}}_{k^-}$  in Proposition 1 with assigned codewords. If the query and the positive key are assigned to different codewords, there will be a large gradient to pull these codewords closer. We find it irreversible without explicit control, because of the insufficient frequency of the same assignment for negative pairs along with subtle gradients to push the same of codewords away. As a result, the representation ability of codebooks degrades and the model degenerates.

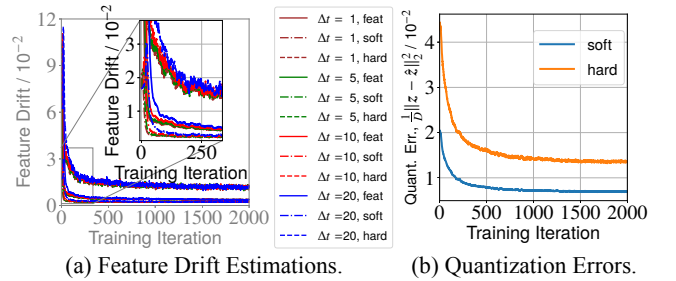


Figure 3: We estimate the feature drifts of original features, soft quantized features, and hard quantized features. The soft features show lower drift than the original features because moderate quantization error can compensate for the drift.

**Codeword Diversity Regularization** To avoid degeneration, we regularize the optimization by imposing  $\Omega_C \leq \epsilon$ , where  $\epsilon$  is a fixed bound. In practice, we set it as a loss term that encourages codeword diversity and guides deep quantization model to pay more attention to proper codeword assignment rather than violently moving the codewords. The blue lines in Figure 2(a) show that the regularization effectively avoids the issue and also helps to calm the loss down.

## Quantization Code Memory to Boost Training

Effective CL methods rely on sufficient negative samples to learn discriminative representations. Therefore, existing memory-based methods cache the image embeddings and serve them as the negatives in the later training. However, as the model keeps updating, the early cached embeddings expire and become noises to CL. To enhance the effect of memory, MoCo (He et al. 2020) introduces a momentum encoder that mitigates the embedding aging issue at a higher computation cost. In contrast, we find an elegant solution that achieves a similar effect more efficiently.

**Feature Drift** We follow Wang et al. (2020) to investigate the embedding aging issue. We define the *feature drift* of a neural embedding model  $h$  by

$$\text{Drift}(\mathcal{X}', t; \Delta t) \triangleq \frac{1}{|\mathcal{X}'|} \sum_{\mathbf{x} \in \mathcal{X}'} \left\| h(\mathbf{x}; \boldsymbol{\theta}_h^t) - h(\mathbf{x}; \boldsymbol{\theta}_h^{t-\Delta t}) \right\|_2^2, \quad (11)$$

where  $\mathcal{X}'$  is a given image set for estimation,  $\boldsymbol{\theta}_h$  is the parameters of  $h$ ,  $t$  and  $\Delta t$  denote the number and the interval of training iterations (*i.e.*, batches) respectively. We train a 32-bit CL-based quantization model and compute its feature drift based on original embeddings, soft quantized reconstructions, and hard quantized reconstructions.

As shown in Figure 3(a), the embeddings violently change at the early stage, after which they become relatively stable. Moreover, it is surprising that the *soft* quantized embeddings show even lower feature drifts than the original embeddings. We realize that undesirable quantization error (illustrated in Figure 3(b)) that used to be eliminated in quantization models *partially*<sup>2</sup> offsets the feature drift, keeping the cached in-

<sup>2</sup>Note that *hard* quantization shows higher feature drift. It doesn't benefit from the offset because of large quantization error.

formation valid for a longer time.

**Memory-augmented Training** Base on the above facts, we start using a memory bank  $\mathcal{M}$  with  $N_{\mathcal{M}}$  slots to store *soft quantization codes* after the warm-up stage. In each training iteration, we fetch the cached codes  $\mathbf{p}_{\mathcal{M}_1}, \mathbf{p}_{\mathcal{M}_2}, \dots, \mathbf{p}_{\mathcal{M}_{N_{\mathcal{M}}}}$  from the memory bank. Then, we forward them to the quantization module and respectively reconstruct the embeddings  $\hat{\mathbf{z}}_{\mathcal{M}_1}, \hat{\mathbf{z}}_{\mathcal{M}_2}, \dots, \hat{\mathbf{z}}_{\mathcal{M}_{N_{\mathcal{M}}}}$  by Eq.(2) and (5). Finally, we integrate these embeddings to Eq.(6) and formulate the memory-augmented loss as

$$\mathcal{L}_{\text{MeCoQ}} = - \sum_{q=1}^{2N} \log \frac{\exp(\frac{s_{q,k+}}{\tau})}{\exp(\frac{s_{q,k+}}{\tau}) + \mathcal{N}_{\text{In-Batch}} + \mathcal{N}_{\text{Memory}}}, \quad (12)$$

where the added negative term about code memory is

$$\mathcal{N}_{\text{Memory}} \triangleq \sum_{i=1}^{N_{\mathcal{M}}} \left[ \frac{\exp(\frac{s_{q,\mathcal{M}_i}}{\tau})}{1 - \rho^+} - \frac{\rho^+ \cdot \exp(\frac{s_{q,k+}}{\tau})}{1 - \rho^+} \right]. \quad (13)$$

At the end of each training iteration, we update the memory as a queue, *i.e.*, the current batch is enqueued and an equal number of the oldest slots are removed. To simplify engineering, we set the queue size  $N_{\mathcal{M}}$  to a multiple of the batch size  $N$  so that we update the memory bank by batches.

## Learning Algorithm

The learning objective of MeCoQ is

$$\min_{\theta_h, \mathcal{C}} \mathbb{E} \mathcal{L}_{\text{MeCoQ}} + \beta \|\theta_h\|_2^2 + \gamma \Omega_{\mathcal{C}}, \quad (14)$$

where  $\mathcal{L}_{\text{MeCoQ}}$  is formulated as Eq.(12),  $\Omega_{\mathcal{C}}$  is defined as Eq.(8).  $\theta_h$  denotes the network parameters of the embedding module  $h$ ,  $\beta$  and  $\gamma$  are the trade-off hyper-parameters. The training process is quite efficient as we formulate the whole problem in a deep learning framework. Many off-the-shelf optimizers can be applied within a few code lines.

## Encoding and Retrieval

In inference, we encode the database with hard quantization:

$$\hat{\mathbf{z}}^m = \arg \max_{\mathbf{c}_i^m \in [\mathbf{c}_1^m, \mathbf{c}_2^m, \dots, \mathbf{c}_K^m]} \mathbf{z}^{m\top} \mathbf{c}_i^m. \quad (15)$$

Given a retrieval query image  $\mathbf{x}_q$ , we extract its deep embedding and cut the vector into  $M$  equal-length segments, *i.e.*,  $\mathbf{z}_q = [\mathbf{z}_q^1; \mathbf{z}_q^2; \dots; \mathbf{z}_q^M]$ ,  $\mathbf{z}_q^m \in \mathbb{R}^d$ . We adopt Asymmetric Quantized Similarity (AQS) (Jegou, Douze, and Schmid 2010) as the metric, which computes the similarity between  $\mathbf{z}_q$  and the reconstruction of a database point  $\hat{\mathbf{z}}_{db}$  by

$$\text{AQS}(\mathbf{x}_q, \mathbf{x}_{db}) = \sum_{m=1}^M \frac{\mathbf{z}_q^{m\top} \hat{\mathbf{z}}_{db}^m}{\|\mathbf{z}_q^m\|_2} = \sum_{m=1}^M \frac{\mathbf{z}_q^{m\top} \mathbf{c}_{i_{db}^m}^m}{\|\mathbf{z}_q^m\|_2}. \quad (16)$$

We can set up a query-specific lookup table  $\Xi_q \in \mathbb{R}^{M \times K}$  for each  $\mathbf{x}_q$ , which stores the pre-computed similarities between the segments of  $\mathbf{x}_q$  and all codewords. Specifically,

$\Xi_{q,i^m}^m = \mathbf{z}_q^{m\top} \mathbf{c}_{i^m}^m / \|\mathbf{z}_q^m\|_2$ . Hence, the AQS can be efficiently computed by summing chosen items from the lookup table according to the quantization code, *i.e.*,

$$\text{AQS}(\mathbf{x}_q, \mathbf{x}_{db}) = \sum_{m=1}^M \Xi_{q,i_{db}^m}^m, \quad (17)$$

where  $i_{db}^m$  is the index of codeword in the  $m$ -th codebook.

## Experiments

### Setup

**Datasets** (i) **Flickr25K** (Huiskes and Lew 2008) contains 25k images from 24 categories. We follow Li and van Gemert (2021) to randomly pick 2,000 images as the testing queries, while another 5,000 images are randomly selected from the rest of the images as the training set. (ii) **CIFAR-10** (Krizhevsky and Hinton 2009) contains 60k images from 10 categories. We consider two typical experiment protocols. *CIFAR-10 (I)*: We follow Li and van Gemert (2021) to use 1k images per class (totally 10k images) as the test query set, and the remaining 50k images are used for training. *CIFAR-10 (II)*: Following Qiu et al. (2021) we randomly select 1,000 images per category as the testing queries and 500 per category as the training set. All images except those in the query set serve as the retrieval database. (iii) **NUS-WIDE** (Chua et al. 2009) is a large-scale image dataset containing about 270k images from 81 categories. We follow Li and van Gemert (2021) to use the 21 most popular categories for evaluation. 100 images per category are randomly selected as the testing queries while the remaining images form the database and the training set.

**Metrics** We adopt the typical metric, Mean Average Precision (**MAP**), from previous works (Yang et al. 2018; Li and van Gemert 2021; Qiu et al. 2021). It is defined as

$$\text{MAP@N} = \frac{1}{|\mathcal{Q}|} \sum_{\mathbf{x}_q \in \mathcal{Q}} \left( \frac{\sum_{n=1}^N \text{Prec}_q(n) \cdot \mathbb{I}_{\{\mathbf{x}_n \in \mathcal{R}_q\}}}{|\mathcal{R}_q|} \right), \quad (18)$$

where  $\mathcal{Q}$  is test query image set and  $n$  is the index of a database image in a returned rank list.  $\text{Prec}_q(n)$  is the precision at cut-off  $n$  in the rank list *w.r.t.*  $\mathbf{x}_q$ .  $\mathcal{R}_q$  is the set of all relevant images *w.r.t.*  $\mathbf{x}_q$ .  $\mathbb{I}_{\{\cdot\}}$  is an indicator function. We follow previous works to adopt MAP@1000 for CIFAR-10 (I) and (II), MAP@5000 for Flickr25K and NUS-WIDE.

**Models** We compare the retrieval performance of **MeCoQ** with 24 classic or state-of-the-art unsupervised baselines, including: (i) 5 shallow hashing methods: **LSH** (Charikar 2002), **SpeH** (Weiss, Torralba, and Fergus 2008), **SH** (Salakhutdinov and Hinton 2009), **SphH** (Heo et al. 2012) and **ITQ** (Gong et al. 2012). (ii) 2 shallow quantization methods: **PQ** (Jegou, Douze, and Schmid 2010) and **OPQ** (Ge et al. 2013). (iii) 15 deep binary hashing methods: **DeepBit** (Lin et al. 2016), **UTH** (Huang et al. 2017), **SAH** (Do et al. 2017), **SGH** (Dai et al. 2017), **HashGAN** (Dizaji et al. 2018), **GreedyHash** (Su et al. 2018), **BinGAN** (Zieba et al. 2018), **BGAN** (Song et al. 2018), **SSDH** (Yang et al. 2018), **DVB** (Shen, Liu, and Shao 2019), **DistillHash** (Yang et al.

Table 1: Mean Average Precision (MAP, %) results for different number of bits on Flickr25K, CIFAR-10 (I and II) and NUS-WIDE datasets. ‘D’, ‘Q’ and ‘BH’ indicate ‘Deep’, ‘Quantization’ and ‘Binary Hashing’ for short in ‘Type’ column.

Method ↓	Dataset →		Flickr25K			CIFAR-10 (I)			CIFAR-10 (II)			NUS-WIDE		
	Venue ↓	Type ↓	16 bits	32 bits	64 bits	16 bits	32 bits	64 bits	16 bits	32 bits	64 bits	16 bits	32 bits	64 bits
LSH+VGG	STOC’02	BH	56.11	57.08	59.26	14.38	15.86	18.09	12.55	13.76	15.07	38.52	41.43	43.89
SpeH+VGG	NeurIPS’08	BH	59.77	61.36	64.08	27.09	29.44	32.65	27.20	28.50	30.00	51.70	51.10	51.00
SH+VGG	IIAR’09	BH	60.02	63.30	64.17	28.28	28.86	28.51	24.68	25.34	27.16	46.85	53.63	56.28
SphH+VGG	CVPR’12	BH	61.32	62.47	64.49	26.90	31.75	35.25	25.40	29.10	33.30	49.50	55.80	58.20
ITQ+VGG	TPAMI’12	BH	63.30	65.92	68.86	34.41	35.41	38.82	30.50	32.50	34.90	62.70	64.50	66.40
PQ+VGG	TPAMI’10	Q	62.75	66.63	69.40	27.14	33.30	37.67	28.16	30.24	30.61	65.39	67.41	68.56
OPQ+VGG	CVPR’13	Q	63.27	68.01	69.86	27.29	35.17	38.48	32.17	33.50	34.46	65.74	68.38	69.12
DeepBit	CVPR’16	DBH	62.04	66.54	68.34	19.43	24.86	27.73	20.60	28.23	31.30	39.20	40.30	42.90
UTH	ACMMM’17	DBH	-	-	-	-	-	-	-	-	-	45.00	49.50	54.90
SAH	CVPR’17	DBH	-	-	-	41.75	45.56	47.36	-	-	-	-	-	-
SGH	ICML’17	DBH	72.10	72.84	72.83	34.51	37.04	38.93	43.50	43.70	43.30	59.30	59.00	60.70
HashGAN	CVPR’18	DBH	72.11	73.25	75.46	44.70	46.30	48.10	42.81	47.54	47.29	68.44	70.56	71.71
GreedyHash	NeurIPS’18	DBH	69.91	70.85	73.03	44.80	47.20	50.10	45.76	48.26	53.34	63.30	69.10	73.10
BinGAN	NeurIPS’18	DBH	-	-	-	-	-	-	47.60	51.20	52.00	65.40	70.90	71.30
BGAN	AAAI’18	DBH	-	-	-	-	-	-	52.50	53.10	56.20	68.40	71.40	73.00
SSDH	IJCAI’18	DBH	75.65	77.10	76.68	36.16	40.37	44.00	33.30	38.29	40.81	58.00	59.30	61.00
DVB	IICV’19	DBH	-	-	-	-	-	-	40.30	42.20	44.60	60.40	63.20	66.50
DistillHash	CVPR’19	DBH	-	-	-	-	-	-	-	-	-	62.70	65.60	67.10
TBH	CVPR’20	DBH	74.38	76.14	77.87	54.68	58.63	62.47	53.20	57.30	57.80	71.70	72.50	73.50
MLS <sup>3</sup> RDUH	IJCAI’20	DBH	-	-	-	-	-	-	-	-	-	71.30	72.70	75.00
Bi-half Net	AAAI’21	DBH	76.07	77.93	78.62	56.10	57.60	59.50	49.97	52.04	55.35	76.86	78.31	79.94
CIBHash	IJCAI’21	DBH	77.21	78.43	79.5	59.39	63.67	65.16	59.00	62.20	64.10	79.00	80.70	81.50
DBD-MQ	CVPR’17	DQ	-	-	-	21.53	26.50	31.85	-	-	-	-	-	-
DeepQuan	IJCAI’18	DQ	-	-	-	39.95	41.25	43.26	-	-	-	-	-	-
MeCoQ (Ours)		DQ	<b>81.31</b>	<b>81.71</b>	<b>82.68</b>	<b>68.20</b>	<b>69.74</b>	<b>71.06</b>	<b>62.88</b>	<b>64.09</b>	<b>65.07</b>	<b>80.18</b>	<b>82.16</b>	<b>83.24</b>

2019), **TBH** (Shen et al. 2020), **MLS<sup>3</sup>RDUH** (Tu, Mao, and Wei 2020), **Bi-half Net** (Li and van Gemert 2021) and **CIBHash** (Qiu et al. 2021). **(iv)** 2 deep quantization methods: **DBD-MQ** (Duan et al. 2017) and **DeepQuan** (Chen, Cheung, and Wang 2018). We carefully collect their results from related literature. When results about some baselines on a certain benchmark are not available (*e.g.* CIBHash on Flickr25K dataset), we try to run their open-sourced codes (*if available and executable*) and report the results.

**Implementation Settings** More details can be found in the Appendix. We implement MeCoQ with Pytorch (Paszke et al. 2019). We follow the standard evaluation protocol (Qiu et al. 2021; Li and van Gemert 2021) of unsupervised deep hashing to use the VGG16 (Simonyan and Zisserman 2015). Specifically, for shallow models, we extract 4096-dimensional deep *fc7* features from each image as the model input. For deep models, we directly use raw image pixels as input and adopt the pre-trained VGG16 (*conv1* ∼ *fc7*) as the backbone network. We use the data augmentation scheme in Qiu et al. (2021) that combines random cropping, horizontal flipping, image graying, and randomly applied color jitter and blur. The default hyper-parameter settings are as follows. **(i)** We set the batch size as 128 and the maximum epoch as 50. **(ii)** The queue length (*i.e.*, the memory bank size),  $N_{\mathcal{M}} = 384$ . **(iii)** The smoothness factor of codeword assignment in Eq.(3),  $\alpha = 10$ . **(iv)** The codeword number of each codebook,  $M = 256$  such that each image is encoded by  $B = M \log_2 K = 8M$  bits (*i.e.*,  $M$  bytes). **(v)** The positive prior,  $\rho^+ = 0.1$  for CIFAR-10 (I and II),  $\rho^+ = 0.15$  for Flickr25K and NUS-WIDE. **(vi)** The start-

ing epoch for the memory module are set to 5 on Flickr25K, 10 on NUS-WIDE and 15 on CIFAR-10 (I and II). Besides, we select hyper-parameters  $\beta, \gamma$  from  $10^{-5}$  to 1.0 and the temperature  $\tau$  from 0.1 to 0.5 via cross-validation.

## Results and Analysis

**Comparison with Existing Methods** The MAP results in Tables 1 show that MeCoQ substantially outperforms all the compared methods. Specifically, compared with CIBHash, a latest and strong baseline, MeCoQ achieves average MAP increases of **3.52**, **6.92**, **2.24** and **1.46** on Flickr25K, CIFAR-10 (I), (II) and NUS-WIDE datasets, respectively. Besides, we can get two findings from the MAP results. **(i)** Deep methods do not always outperform shallow methods with CNN features. For instance, DeepBit and UTH do not outperform PQ and OPQ with CNN features on NUS-WIDE. It implies that without label supervision, some deep hashing methods are less effective to take good advantage of pre-trained CNNs. **(ii)** Contrastive Learning (CL) is effective to learn deep hashing models. The two CL-based methods in Table 1, CIBHash and MeCoQ, perform best on all datasets. Moreover, with debiasing mechanism and code memory, MeCoQ shows notable improvements over CIBHash.

**Component Analysis** We set 6 MeCoQ variants to analyse the contributions of components: **(i)** MeCoQ <sub>w/o</sub> debiasing removes debiasing mechanism by setting  $\rho^+ = 0$  in Eq.(7) and (13); **(ii)** MeCoQ <sub>w/o</sub>  $\Omega_{\mathcal{C}}$  removes codeword regularization,  $\Omega_{\mathcal{C}}$ ; **(iii)** MeCoQ <sub>w/o</sub>  $\mathcal{M}$  removes the code memory,  $\mathcal{M}$ ; **(iv)** MeCoQ <sub>feature</sub>  $\mathcal{M}$  replaces soft code memory by feature memory; **(v)** MeCoQ <sub>hard code</sub>  $\mathcal{M}$  replaces soft code mem-

Table 2: Mean Average Precision (MAP, %) results for different MeCoQ variants with different number of bits on Flickr25K, CIFAR-10 (I and II) and NUS-WIDE datasets. The subscript results are the MAP drops compared with full MeCoQ.

Dataset $\rightarrow$	Flickr25K			CIFAR-10 (I)			CIFAR-10 (II)			NUS-WIDE		
	16 bits	32 bits	64 bits	16 bits	32 bits	64 bits	16 bits	32 bits	64 bits	16 bits	32 bits	64 bits
MeCoQ	<b>81.31</b>	<b>81.71</b>	<b>82.68</b>	<b>68.20</b>	<b>69.74</b>	<b>71.06</b>	<b>62.88</b>	<b>64.09</b>	<b>65.07</b>	<b>80.18</b>	<b>82.16</b>	<b>83.24</b>
MeCoQ w/o debiasing	80.03( $\downarrow$ 1.28)	80.19( $\downarrow$ 1.52)	80.67( $\downarrow$ 2.01)	66.59( $\downarrow$ 1.61)	67.08( $\downarrow$ 2.66)	68.77( $\downarrow$ 2.29)	60.51( $\downarrow$ 2.37)	62.81( $\downarrow$ 1.28)	62.85( $\downarrow$ 2.22)	79.64( $\downarrow$ 0.54)	80.68( $\downarrow$ 1.48)	82.30( $\downarrow$ 0.94)
MeCoQ w/o $\Omega_C$	54.00( $\downarrow$ 27.31)	57.53( $\downarrow$ 24.18)	58.84( $\downarrow$ 23.84)	39.03( $\downarrow$ 29.17)	36.20( $\downarrow$ 33.54)	42.75( $\downarrow$ 28.31)	32.54( $\downarrow$ 30.34)	35.67( $\downarrow$ 28.42)	36.40( $\downarrow$ 28.67)	51.33( $\downarrow$ 28.85)	57.29( $\downarrow$ 24.87)	61.01( $\downarrow$ 22.23)
MeCoQ w/o $\mathcal{M}$	78.77( $\downarrow$ 2.54)	79.50( $\downarrow$ 2.21)	80.76( $\downarrow$ 1.92)	64.82( $\downarrow$ 3.38)	67.64( $\downarrow$ 2.10)	69.36( $\downarrow$ 1.70)	59.78( $\downarrow$ 3.10)	61.22( $\downarrow$ 2.87)	63.80( $\downarrow$ 1.27)	76.70( $\downarrow$ 3.48)	79.13( $\downarrow$ 3.03)	81.43( $\downarrow$ 1.81)
MeCoQ feature $\mathcal{M}$	78.39( $\downarrow$ 2.92)	79.61( $\downarrow$ 2.10)	80.13( $\downarrow$ 2.55)	65.39( $\downarrow$ 2.81)	67.62( $\downarrow$ 2.12)	70.57( $\downarrow$ 0.49)	62.55( $\downarrow$ 0.33)	63.32( $\downarrow$ 0.77)	64.84( $\downarrow$ 0.23)	77.71( $\downarrow$ 2.47)	79.90( $\downarrow$ 2.26)	81.64( $\downarrow$ 1.60)
MeCoQ hard code $\mathcal{M}$	60.77( $\downarrow$ 20.54)	63.10( $\downarrow$ 18.61)	68.49( $\downarrow$ 14.19)	33.95( $\downarrow$ 34.25)	40.65( $\downarrow$ 29.09)	46.76( $\downarrow$ 24.30)	34.40( $\downarrow$ 28.48)	37.55( $\downarrow$ 26.54)	44.90( $\downarrow$ 20.17)	69.46( $\downarrow$ 10.72)	72.23( $\downarrow$ 9.93)	74.95( $\downarrow$ 8.29)
MeCoQ w/o delaying $\mathcal{M}$	79.02( $\downarrow$ 2.29)	78.44( $\downarrow$ 3.27)	78.17( $\downarrow$ 4.51)	66.76( $\downarrow$ 1.44)	67.82( $\downarrow$ 1.92)	69.04( $\downarrow$ 2.02)	59.79( $\downarrow$ 3.09)	61.42( $\downarrow$ 2.67)	62.60( $\downarrow$ 2.47)	79.72( $\downarrow$ 0.46)	81.39( $\downarrow$ 0.77)	82.67( $\downarrow$ 0.57)

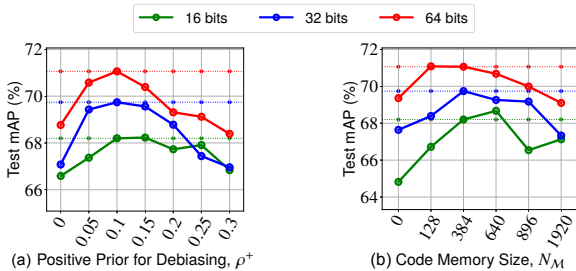


Figure 4: Sensitivities of  $\rho^+$  and  $N_M$  on CIFAR-10 (I). The dotted lines indicate the MAP results of default settings.

emory by hard code memory; (vi) MeCoQ w/o delaying  $\mathcal{M}$  begins memory-augmented training at the very start of the learning. We can make the following summaries based on the Table 2.

**Debiasing improves performance.** MeCoQ outperforms MeCoQ w/o debiasing by 1.60, 2.19, 1.96 and 0.99 of average MAPs on Flickr25K, CIFAR-10 (I), (II) and NUS-WIDE, which shows that correcting the sampling bias can improve model training. Figure 4(a) shows that the optimal  $\rho^+$  on CIFAR-10 (I) is about 0.1, which means that we may randomly drop a false-negative sample from the training set with a 10% probability. It is consistent with the property of CIFAR-10 (I) that each category accounts for 10%.

**The codeword diversity regularization avoids model degeneration.** MeCoQ outperforms MeCoQ w/o  $\Omega_C$  by 25.11, 30.34, 29.14 and 25.32 of average MAPs on 4 datasets. It demonstrates the importance of regularization.

**Soft code memory is effective and efficient to enhance contrastive learning.** MeCoQ outperforms MeCoQ w/o  $\mathcal{M}$  by 2.22, 2.39, 2.41 and 2.77 of average MAPs on 4 datasets, which verifies the worth of using  $\mathcal{M}$ . Besides, Figure 4(b) shows that enlarging memory to cache more negatives improves MeCoQ, while the improvement tends to drop as memory size exceeds a certain range. The reason is that the low feature drift phenomenon only holds within a limited period. We can also learn that fewer bits with larger quantization errors allow a slightly larger memory because the quantization error can partially offset the feature drift. Moreover, as shown in Table 3, using code memory is efficient in GPU memory and computation. It can achieve better results with much less GPU memory than enlarging batch size. The marginal increase of time is caused by similarity computations between training queries and cached negatives.

**Soft code memory is better than feature memory and**

Table 3: Model profiling results on CIFAR-10 (I) dataset, including the number of negative samples ('#Neg.') per training query, average training time per epoch in seconds ('Time / Ep. / sec'), GPU memory demand in megabytes ('GPU Mem. / MB') and MAP (%) for 32 bits, under different batch size and memory size settings.  $N$  and  $N_M$  denote the batch size and memory size respectively. We do these experiments on a single NVIDIA GeForce GTX 1080 Ti (11GB) and Intel® Xeon® CPU E5-2650 v4 @ 2.20GHz (48 cores).

Method	#Neg.	Time / Ep. / sec	GPU Mem. / MB	MAP(%)@32 bits
$N=128$ , w/o $\mathcal{M}$	128	528	5925	67.64
$N=256$ , w/o $\mathcal{M}$	256	550( $\uparrow$ 22)	10927( $\uparrow$ 5002)	68.66( $\uparrow$ 1.02)
$N=128$ , $N_M=128$	256	536( $\uparrow$ 8)	5927( $\uparrow$ 2)	68.39( $\uparrow$ 0.75)
$N=128$ , $N_M=384$	512	547( $\uparrow$ 19)	5933( $\uparrow$ 8)	69.74( $\uparrow$ 2.10)
$N=128$ , $N_M=896$	1024	563( $\uparrow$ 35)	5947( $\uparrow$ 22)	69.17( $\uparrow$ 1.53)

**hard code memory.** MeCoQ outperforms MeCoQ feature  $\mathcal{M}$  by 2.52, 1.81, 0.44 and 2.11 of average MAPs on 4 datasets, because the soft code memory has lower feature drift than feature memory. Surprisingly, MeCoQ hard code  $\mathcal{M}$  fails. It seems that reconstructed features from hard codes become adverse noises rather than valid negatives because the large error of hard quantization leads to an over-large feature drift.

**It is better to delay the usage of memory in the learning process.** MeCoQ outperforms MeCoQ w/o delaying  $\mathcal{M}$  by 3.36, 1.79, 2.74 and 0.6 of average MAPs on 4 datasets. It implies that using code memory from the very beginning leads to sub-optimal solutions because reusing unstable representations in initial training stage is not recommended.

## Conclusions

In this paper, we propose **Contrastive Quantization with Code Memory (MeCoQ)** for unsupervised deep quantization. Different from existing reconstruction-based unsupervised deep hashing methods, MeCoQ learns quantization by contrastive learning. To avoid model degeneration when optimizing MeCoQ, we introduce a codeword diversity regularization. We further improve the memory-based contrastive learning by designing a novel quantization code memory, which shows lower feature drift than existing feature memories without using momentum encoder. Extensive experiments show the superiority of MeCoQ over the state-of-the-art methods. More importantly, MeCoQ sheds light on a promising future direction to unsupervised deep hashing. Potentials of contrastive learning remain to be explored.

## Appendix

### Proof of Proposition 1

**Proposition 2.** Suppose that  $\mathbf{x}_{k^+}$  is the positive training key and  $\mathbf{x}_{k^-}$  is a negative key to  $\mathbf{x}_q$ .  $\hat{\mathbf{z}}_{k^+}$  and  $\hat{\mathbf{z}}_{k^-}$  are the reconstructed embeddings w.r.t.  $\mathbf{x}_{k^+}$  and  $\mathbf{x}_{k^-}$ , then we have

$$\left\| \frac{\partial \mathcal{L}_{\text{CL}}(\mathbf{x}_q)}{\partial \hat{\mathbf{z}}_{k^+}} \right\| > \left\| \frac{\partial \mathcal{L}_{\text{CL}}(\mathbf{x}_q)}{\partial \hat{\mathbf{z}}_{k^-}} \right\| > 0. \quad (19)$$

*Proof.* The contrastive learning loss w.r.t.  $\mathbf{x}_q$  is

$$\mathcal{L}_{\text{CL}}(\mathbf{x}_q) = -\log \frac{\exp(\frac{s_{q,k^+}}{\tau})}{\exp(\frac{s_{q,k^+}}{\tau}) + \sum_{\substack{k^-=1, \\ k^- \notin \{q, k^+\}}}^{2N} \exp(\frac{s_{q,k^-}}{\tau})}, \quad (20)$$

where  $\tau$  is the temperature hyper-parameter. The similarity between a query  $\mathbf{x}_q$  and a key  $\mathbf{x}_k$  is defined as  $s_{q,k} \triangleq \hat{\mathbf{z}}_q^\top \hat{\mathbf{z}}_k$ .

Then, the loss gradient w.r.t. the similarity score  $s_{q,k}$  is

$$\frac{\partial \mathcal{L}_{\text{CL}}(\mathbf{x}_q)}{\partial s_{q,k}} = \begin{cases} -\frac{1}{\tau} \sum_{\substack{k^-=1, \\ k^- \notin \{q, k^+\}}}^{2N} P_{q,k^-}, & k = k^+, \\ \frac{1}{\tau} P_{q,k}, & k \neq k^+, \end{cases} \quad (21)$$

where  $P_{q,k}$  is the probability that  $\mathbf{x}_k$  is a positive key to  $\mathbf{x}_q$ :

$$P_{q,k} = \frac{\exp(\frac{s_{q,k}}{\tau})}{\exp(\frac{s_{q,k^+}}{\tau}) + \sum_{\substack{k^-=1, \\ k^- \notin \{q, k^+\}}}^{2N} \exp(\frac{s_{q,k^-}}{\tau})}. \quad (22)$$

We can learn from Eq.(21) that the magnitude of gradient w.r.t. the positive score is equal to the sum of those w.r.t. all negative scores, i.e.,

$$\left| \frac{\partial \mathcal{L}_{\text{CL}}(\mathbf{x}_q)}{\partial s_{q,k^+}} \right| \equiv \sum_{\substack{k^-=1, \\ k^- \notin \{q, k^+\}}}^{2N} \left| \frac{\partial \mathcal{L}_{\text{CL}}(\mathbf{x}_q)}{\partial s_{q,k^-}} \right|. \quad (23)$$

Therefore, we can get the norm of loss gradient w.r.t. the soft quantized features of positive key by

$$\left\| \frac{\partial \mathcal{L}_{\text{CL}}(\mathbf{x}_q)}{\partial \hat{\mathbf{z}}_{k^+}} \right\| = \left\| \frac{\partial \mathcal{L}_{\text{CL}}(\mathbf{x}_q)}{\partial s_{q,k^+}} \cdot \frac{\partial s_{q,k^+}}{\partial \hat{\mathbf{z}}_{k^+}} \right\| \quad (24)$$

$$= \left\| \frac{\partial \mathcal{L}_{\text{CL}}(\mathbf{x}_q)}{\partial s_{q,k^+}} \right\| \left\| \frac{\partial s_{q,k^+}}{\partial \hat{\mathbf{z}}_{k^+}} \right\| \quad (25)$$

$$= \left\| \frac{\partial \mathcal{L}_{\text{CL}}(\mathbf{x}_q)}{\partial s_{q,k^+}} \right\| \left\| \hat{\mathbf{z}}_q \right\| \quad (26)$$

$$= \sum_{\substack{k^-=1, \\ k^- \notin \{q, k^+\}}}^{2N} \left( \left\| \frac{\partial \mathcal{L}_{\text{CL}}(\mathbf{x}_q)}{\partial s_{q,k^-}} \right\| \left\| \hat{\mathbf{z}}_q \right\| \right) \quad (27)$$

$$= \sum_{\substack{k^-=1, \\ k^- \notin \{q, k^+\}}}^{2N} \left( \left\| \frac{\partial \mathcal{L}_{\text{CL}}(\mathbf{x}_q)}{\partial s_{q,k^-}} \right\| \left\| \frac{\partial s_{q,k^-}}{\partial \hat{\mathbf{z}}_{k^-}} \right\| \right) \quad (28)$$

$$= \sum_{\substack{k^-=1, \\ k^- \notin \{q, k^+\}}}^{2N} \left\| \frac{\partial \mathcal{L}_{\text{CL}}(\mathbf{x}_q)}{\partial \hat{\mathbf{z}}_{k^-}} \right\|. \quad (29)$$

Table 4: The computing infrastructure for our experiments.

Name	Configuration
CPU	Intel® Xeon® CPU E5-2650 v4 @ 2.20GHz (48 cores)
GPU	A single NVIDIA GeForce GTX 1080 Ti (11GB)
RAM	64GB
OS	Ubuntu 16.04.4 LTS
CUDA Version	10.1
GPU Driver Version	430.50
Language	Python 3.7.9
Dependencies	
cudnn 7.6.5	
torch 1.3.1	
torchvision 0.4.2	
numpy 1.19.1	
opencv-python 3.4.2	
pillow 8.0.0	

Besides, since

$$\forall \mathbf{x}_q : \|\hat{\mathbf{z}}_q\| > 0, \quad \forall \mathbf{x}_{k^-} : \frac{\partial \mathcal{L}_{\text{CL}}(\mathbf{x}_q)}{\partial \hat{\mathbf{z}}_{k^-}} = \frac{1}{\tau} P_{q,k^-} > 0, \quad (30)$$

we have

$$\left\| \frac{\partial \mathcal{L}_{\text{CL}}(\mathbf{x}_q)}{\partial \hat{\mathbf{z}}_{k^-}} \right\| > 0. \quad (31)$$

Combining Eq.(29) and (31), we come to the conclusion that

$$\left\| \frac{\partial \mathcal{L}_{\text{CL}}(\mathbf{x}_q)}{\partial \hat{\mathbf{z}}_{k^+}} \right\| > \left\| \frac{\partial \mathcal{L}_{\text{CL}}(\mathbf{x}_q)}{\partial \hat{\mathbf{z}}_{k^-}} \right\| > 0. \quad (32)$$

□

## Computing Infrastructure for Experiments

We list the computing infrastructure in Table 4.

## Additional Experiments

**Parameter Sensitivity** We evaluate the sensitivities of different hyper-parameters in MeCoQ.

As shown in Figure 5(a)-(d), for each bit-length on each dataset, there is a memory size that brings the maximum gain. When the memory size exceeds this value, the gain tends to drop, because the low feature drift phenomenon only holds within a limited period. Because of the larger quantization errors to offset the feature drift, a lower bit-length quantization model empirically benefits most from a larger code memory.

Figure 5(e)-(h) shows the sensitivity of smoothing factor  $\alpha$  in soft quantization. As  $\alpha \rightarrow \infty$ , the  $\alpha$ -softmax (Eq.(3)) converges to argmax and reduces the gap between soft quantization and hard quantization. However, as  $\alpha$  enlarges, the gradients w.r.t. the non-primary assigned codewords vanish, making it hard to optimize the model. On the other hand, as  $\alpha \rightarrow 0$ , the soft codeword assignments in training vary too much from the hard assignments in inference, also leading to inferior results. We observe that a promising  $\alpha$  for MeCoQ is about 10.

As shown in Figure 5(i)-(l), the positive prior  $\rho^+$  helps to correct the sampling bias and improve the retrieval performance. The best setting is dataset-specific. Empirically,

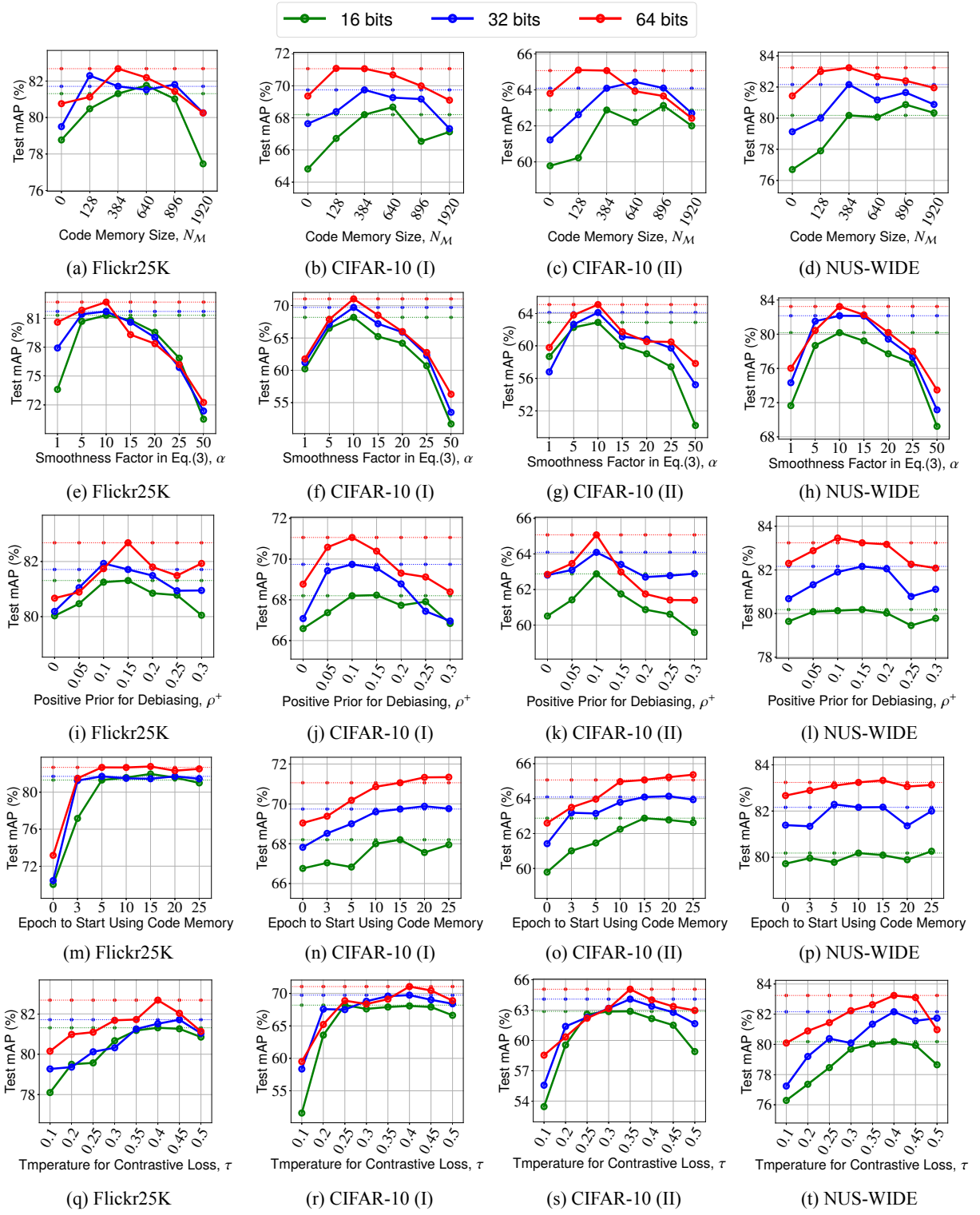


Figure 5: Parameter sensitivities. The dotted lines indicate the MAP results of default settings.

the model performs best when  $\rho^+ = 0.1$  on CIFAR-10 and  $\rho^+ = 0.15$  on Flickr25K and NUS-WIDE.

We can learn from Figure 5(m)-(p) that delaying the usage

of code memory in training is important to make the best of it. As the embeddings are unstable at the beginning of the training, it is recommended to use code memory after about

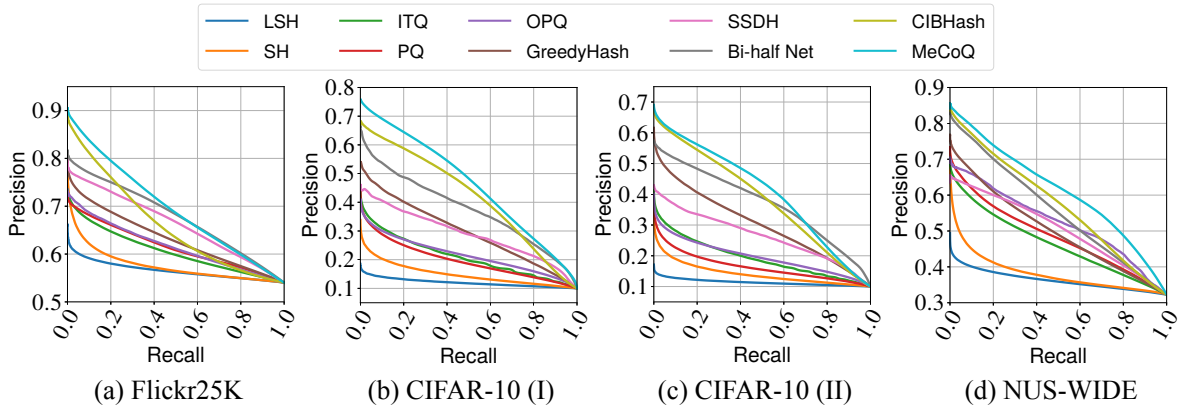


Figure 6: Precision-Recall curves on the Flickr25K, CIFAR-10 (I), CIFAR-10 (II) and NUS-WIDE at 64 bits.

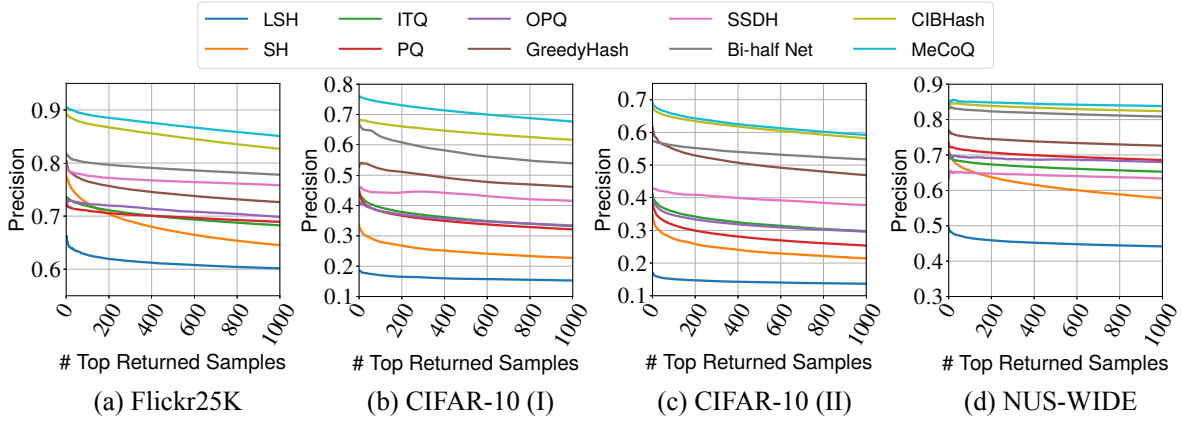


Figure 7: Precision@top- $N$  ( $N \leq 1000$ ) curves on the Flickr25K, CIFAR-10 (I), CIFAR-10 (II) and NUS-WIDE at 64 bits.

5 epochs on Flickr25K and after about 10 epochs on CIFAR-10 and NUS-WIDE.

Figure 5(q)-(t) shows that a proper temperature  $\tau$  is important to the effect of contrastive learning. It controls the strength of penalties on negative samples (Wang and Liu 2021). Empirically, we observe that  $0.35 \sim 0.45$  is a reasonable range for  $\tau$ .

**Precision-Recall and Precision@top- $N$  Curves** The Precision-Recall and Precision@top- $N$  curves on 4 datasets are shown in Figure 6 and 7. The proposed MeCoQ outperforms other baselines, demonstrating that contrastive learning help to learn better representations for retrieval.

**Visualization** For a better understanding, we show the t-SNE visualization of deep representations produced by Bi-half Net, CIBHash, and MeCoQ in Figure 8. We can learn that the representations produced by MeCoQ have a clearer structure. For example, the clusters of categories *trucks* and *cars* can be discriminated from MeCoQ, while those of Bi-half Net and CIBHash are mixed. Besides, compared with CIBHash, MeCoQ produces more compact clusters with clearer boundaries for categories *ships*, *trucks* and *cars*, which demonstrates that the code memory and the debiasing mechanism in MeCoQ help to enhance contrastive learning

and generate more discriminative representations.

We also illustrate some representative cases of top-10 images returned by MeCoQ, CIBHash and Bi-half Net. As shown in Figure 9, MeCoQ returns more relevant results than CIBHash and Bi-half Net.

## References

- Caron, M.; Misra, I.; Mairal, J.; Goyal, P.; Bojanowski, P.; and Joulin, A. 2020. Unsupervised Learning of Visual Features by Contrasting Cluster Assignments. In *Thirty-fourth Conference on Neural Information Processing Systems (NeurIPS)*.
- Charikar, M. S. 2002. Similarity estimation techniques from rounding algorithms. In *Proceedings of the thirty-fourth annual ACM symposium on Theory of computing*, 380–388.
- Chen, J.; Cheung, W. K.; and Wang, A. 2018. Learning Deep Unsupervised Binary Codes for Image Retrieval. In *IJCAI*, 613–619.
- Chen, T.; Kornblith, S.; Norouzi, M.; and Hinton, G. 2020. A simple framework for contrastive learning of visual representations. In *International conference on machine learning*, 1597–1607. PMLR.
- Chua, T.-S.; Tang, J.; Hong, R.; Li, H.; Luo, Z.; and Zheng,

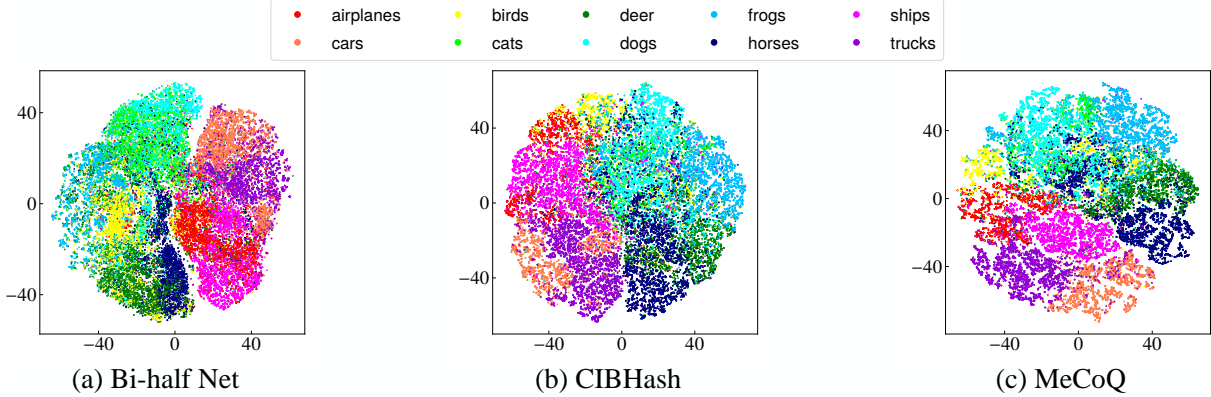


Figure 8: The t-SNE visualizations of representations learned by Bi-half Net, CIBHash and MeCoQ on CIFAR-10 (I) at 64 bits.

Y. 2009. Nus-wide: a real-world web image database from national university of singapore. In *Proceedings of the ACM international conference on image and video retrieval*, 1–9.

Chuang, C.-Y.; Robinson, J.; Lin, Y.-C.; Torralba, A.; and Jegelka, S. 2020. Debiased Contrastive Learning. In *Advances in Neural Information Processing Systems*, volume 33, 8765–8775.

Dai, B.; Guo, R.; Kumar, S.; He, N.; and Song, L. 2017. Stochastic generative hashing. In *International Conference on Machine Learning*, 913–922. PMLR.

Dizaji, K. G.; Zheng, F.; Sadoughi, N.; Yang, Y.; Deng, C.; and Huang, H. 2018. Unsupervised deep generative adversarial hashing network. In *Proceedings of the IEEE Conference on Computer Vision and Pattern Recognition*, 3664–3673.

Do, T.-T.; Le Tan, D.-K.; Pham, T. T.; and Cheung, N.-M. 2017. Simultaneous feature aggregating and hashing for large-scale image search. In *Proceedings of the IEEE Conference on Computer Vision and Pattern Recognition*, 6618–6627.

Duan, Y.; Lu, J.; Wang, Z.; Feng, J.; and Zhou, J. 2017. Learning deep binary descriptor with multi-quantization. In *Proceedings of the IEEE conference on computer vision and pattern recognition*, 1183–1192.

Ge, T.; He, K.; Ke, Q.; and Sun, J. 2013. Optimized product quantization for approximate nearest neighbor search. In *Proceedings of the IEEE Conference on Computer Vision and Pattern Recognition*, 2946–2953.

Gong, Y.; Lazebnik, S.; Gordo, A.; and Perronnin, F. 2012. Iterative quantization: A procrustean approach to learning binary codes for large-scale image retrieval. *IEEE transactions on pattern analysis and machine intelligence*, 35(12): 2916–2929.

Hadsell, R.; Chopra, S.; and LeCun, Y. 2006. Dimensionality reduction by learning an invariant mapping. In *IEEE Computer Society Conference on Computer Vision and Pattern Recognition (CVPR)*, volume 2, 1735–1742. IEEE.

He, K.; Fan, H.; Wu, Y.; Xie, S.; and Girshick, R. 2020. Momentum contrast for unsupervised visual representation learning. In *Proceedings of the IEEE/CVF Conference on Computer Vision and Pattern Recognition*, 9729–9738.

He, K.; Zhang, X.; Ren, S.; and Sun, J. 2016. Deep residual learning for image recognition. In *Proceedings of the IEEE conference on computer vision and pattern recognition*, 770–778.

Heo, J.-P.; Lee, Y.; He, J.; Chang, S.-F.; and Yoon, S.-E. 2012. Spherical hashing. In *2012 IEEE Conference on Computer Vision and Pattern Recognition*, 2957–2964. IEEE.

Huang, S.; Xiong, Y.; Zhang, Y.; and Wang, J. 2017. Unsupervised triplet hashing for fast image retrieval. In *Proceedings of the on Thematic Workshops of ACM Multimedia 2017*, 84–92.

Huiskes, M. J.; and Lew, M. S. 2008. The mir flickr retrieval evaluation. In *Proceedings of the 1st ACM international conference on Multimedia information retrieval*, 39–43.

Jegou, H.; Douze, M.; and Schmid, C. 2010. Product quantization for nearest neighbor search. *IEEE transactions on pattern analysis and machine intelligence*, 33(1): 117–128.

Krizhevsky, A.; and Hinton, G. 2009. Learning multiple layers of features from tiny images. Technical report, University of Toronto, Toronto, Ontario.

Krizhevsky, A.; Sutskever, I.; and Hinton, G. E. 2012. Imagenet classification with deep convolutional neural networks. In *Advances in neural information processing systems (NIPS)*, volume 25, 1097–1105.

Li, J.; Zhou, P.; Xiong, C.; and Hoi, S. 2021. Prototypical Contrastive Learning of Unsupervised Representations. In *International Conference on Learning Representations*.

Li, Y.; and van Gemert, J. 2021. Deep Unsupervised Image Hashing by Maximizing Bit Entropy. In *Proceedings of the AAAI Conference on Artificial Intelligence*.

Lin, K.; Lu, J.; Chen, C.-S.; and Zhou, J. 2016. Learning compact binary descriptors with unsupervised deep neural networks. In *Proceedings of the IEEE conference on computer vision and pattern recognition*, 1183–1192.

Liu, H.; Wang, R.; Shan, S.; and Chen, X. 2016. Deep supervised hashing for fast image retrieval. In *Proceedings of the IEEE conference on computer vision and pattern recognition*, 2064–2072.

Lowe, D. G. 2004. Distinctive image features from scale-invariant keypoints. *International journal of computer vision*, 60(2): 91–110.

Misra, I.; and Maaten, L. v. d. 2020. Self-supervised learning of pretext-invariant representations. In *Proceedings of the IEEE/CVF Conference on Computer Vision and Pattern Recognition*, 6707–6717.

Morozov, S.; and Babenko, A. 2019. Unsupervised neural quantization for compressed-domain similarity search. In *Proceedings of the IEEE/CVF International Conference on Computer Vision*, 3036–3045.

Oliva, A.; and Torralba, A. 2001. Modeling the shape of the scene: A holistic representation of the spatial envelope. *International journal of computer vision*, 42(3): 145–175.

Oord, A. v. d.; Li, Y.; and Vinyals, O. 2018. Representation learning with contrastive predictive coding. *arXiv preprint arXiv:1807.03748*.

Paszke, A.; Gross, S.; Massa, F.; Lerer, A.; Bradbury, J.; Chanan, G.; Killeen, T.; Lin, Z.; Gimelshein, N.; Antiga, L.; et al. 2019. PyTorch: An imperative style, high-performance deep learning library. In *NeurIPS*, 8024–8035.

Qiu, Z.; Su, Q.; Ou, Z.; Yu, J.; and Chen, C. 2021. Unsupervised Hashing with Contrastive Information Bottleneck. In *IJCAI*.

Robinson, J. D.; Chuang, C.-Y.; Sra, S.; and Jegelka, S. 2021. Contrastive Learning with Hard Negative Samples. In *International Conference on Learning Representations*.

Salakhutdinov, R.; and Hinton, G. 2009. Semantic hashing. *International Journal of Approximate Reasoning*, 50(7): 969–978.

Shen, F.; Xu, Y.; Liu, L.; Yang, Y.; Huang, Z.; and Shen, H. T. 2018. Unsupervised deep hashing with similarity-adaptive and discrete optimization. *IEEE transactions on pattern analysis and machine intelligence*, 40(12): 3034–3044.

Shen, Y.; Liu, L.; and Shao, L. 2019. Unsupervised binary representation learning with deep variational networks. *International Journal of Computer Vision*, 127(11): 1614–1628.

Shen, Y.; Qin, J.; Chen, J.; Yu, M.; Liu, L.; Zhu, F.; Shen, F.; and Shao, L. 2020. Auto-encoding twin-bottleneck hashing. In *Proceedings of the IEEE/CVF Conference on Computer Vision and Pattern Recognition*, 2818–2827.

Simonyan, K.; and Zisserman, A. 2015. Very Deep Convolutional Networks for Large-Scale Image Recognition. In *3rd International Conference on Learning Representations, ICLR*.

Song, J.; He, T.; Gao, L.; Xu, X.; Hanjalic, A.; and Shen, H. T. 2018. Binary generative adversarial networks for image retrieval. In *Thirty-second AAAI conference on artificial intelligence*.

Su, S.; Zhang, C.; Han, K.; and Tian, Y. 2018. Greedy hash: Towards fast optimization for accurate hash coding in cnn. In *Proceedings of the 32nd International Conference on Neural Information Processing Systems*, 806–815.

Tu, R.-C.; Mao, X.-L.; and Wei, W. 2020. MLS3RDUH: Deep Unsupervised Hashing via Manifold based Local Semantic Similarity Structure Reconstructing. In *Proceedings of the Twenty-Ninth International Joint Conference on Artificial Intelligence*, 3466–3472.

Wang, F.; and Liu, H. 2021. Understanding the Behaviour of Contrastive Loss. In *IEEE conference on computer vision and pattern recognition (to appear)*.

Wang, J.; Zhang, T.; Sebe, N.; Shen, H. T.; et al. 2017. A survey on learning to hash. *IEEE transactions on pattern analysis and machine intelligence*, 40(4): 769–790.

Wang, X.; Zhang, H.; Huang, W.; and Scott, M. R. 2020. Cross-batch memory for embedding learning. In *Proceedings of the IEEE/CVF Conference on Computer Vision and Pattern Recognition*, 6388–6397.

Weiss, Y.; Torralba, A.; and Fergus, R. 2008. Spectral hashing. In *22nd Annual Conference on Neural Information Processing Systems*, 1753–1760.

Wu, Z.; Xiong, Y.; Yu, S. X.; and Lin, D. 2018. Unsupervised feature learning via non-parametric instance discrimination. In *Proceedings of the IEEE Conference on Computer Vision and Pattern Recognition*, 3733–3742.

Yang, E.; Deng, C.; Liu, T.; Liu, W.; and Tao, D. 2018. Semantic structure-based unsupervised deep hashing. In *Proceedings of the 27th International Joint Conference on Artificial Intelligence*, 1064–1070.

Yang, E.; Liu, T.; Deng, C.; Liu, W.; and Tao, D. 2019. Distillhash: Unsupervised deep hashing by distilling data pairs. In *Proceedings of the IEEE/CVF Conference on Computer Vision and Pattern Recognition*, 2946–2955.

Yuan, L.; Wang, T.; Zhang, X.; Tay, F. E.; Jie, Z.; Liu, W.; and Feng, J. 2020. Central similarity quantization for efficient image and video retrieval. In *Proceedings of the IEEE/CVF Conference on Computer Vision and Pattern Recognition*, 3083–3092.

Zhang, T.; Du, C.; and Wang, J. 2014. Composite quantization for approximate nearest neighbor search. In *International Conference on Machine Learning*, 838–846. PMLR.

Zieba, M.; Semberecki, P.; El-Gaaly, T.; and Trzcinski, T. 2018. BinGAN: learning compact binary descriptors with a regularized GAN. In *Proceedings of the 32nd International Conference on Neural Information Processing Systems*, 3612–3622.

Query	Top 10 Retrieved Image									
Flickr25K  flower	         	✓	✓	✓	✓	✓	✓	✓	✓	✓
	         	✓	✓	✓	✓	✓	✓	✓	✓	✓
	         	✓	✓	✓	✓	✓	✓	✗	✓	✓
	         	✓	✓	✗	✓	✓	✓	✓	✓	✓
	         	✓	✓	✗	✓	✓	✓	✓	✓	✓
CIFAR-10 (I)  automobile	         	✓	✓	✓	✓	✓	✓	✓	✗	✓
	         	✓	✓	✓	✓	✓	✓	✓	✓	✓
	         	✓	✓	✓	✗	✓	✗	✓	✓	✓
	         	✓	✗	✓	✓	✓	✗	✓	✓	✓
	         	✓	✗	✓	✓	✓	✓	✓	✗	✓
CIFAR-10 (II)  cat	         	✓	✓	✓	✓	✓	✗	✓	✓	✓
	         	✓	✓	✓	✓	✓	✓	✗	✓	✓
	         	✓	✓	✓	✗	✓	✓	✗	✓	✓
	         	✓	✗	✓	✓	✓	✓	✗	✓	✓
	         	✓	✗	✓	✓	✓	✓	✗	✓	✓
NUS-WIDE  buildings	         	✓	✓	✓	✓	✓	✓	✓	✓	✓
	         	✓	✓	✓	✓	✓	✓	✓	✓	✓
	         	✓	✓	✓	✓	✗	✓	✓	✓	✓
	         	✓	✓	✓	✗	✓	✓	✗	✓	✓
	         	✓	✓	✓	✓	✓	✓	✓	✓	✓

Figure 9: The top-10 images returned by Bi-half Net, CIBHash and MeCoQ at 64 bits.